The Imprint of Primary Production on High-Frequency Profiles of Lake Optical Properties

Camille Minaudo,* Daniel Odermatt, Damien Bouffard, Abolfazl Irani Rahaghi, Sébastien Lavanchy, and Alfred Wüest

Read Online

ACCESS | Metrics & More | Article Recommendations | Supporting Information

ABSTRACT: Water inherent optical properties (IOPs) contain integrative information on the optical constituents of surface waters. In lakes, IOP measurements have not been traditionally collected. This study describes how high-frequency IOP profiles can be used to document short-term physical and biogeochemical processes that ultimately influence the long-term trajectory of lake ecosystems. Between October 2018 and May 2020, we collected 1373 high-resolution hyperspectral IOP profiles in the uppermost 50 m of the large mesotrophic Lake Geneva (Switzerland—France), using an autonomous profiler. A data set of this size and content does not exist for any other lake. Results showed seasonal variations in the IOPs, following the expected dynamic of phytoplankton. We found systematic diel patterns in the IOPs. Phases of these diel cycles were consistent year-round, and amplitudes correlated to the diurnal variations of dissolved oxygen, clarifying the link between IOPs and phytoplankton metabolism. Diel amplitudes were largest in spring and summer under low wind condition. Wind-driven changes in thermal stratification impacted the dynamic of the IOPs, illustrating the potential of high-frequency profiles of water optical properties to increase our understanding of carbon cycling in lake ecosystems.
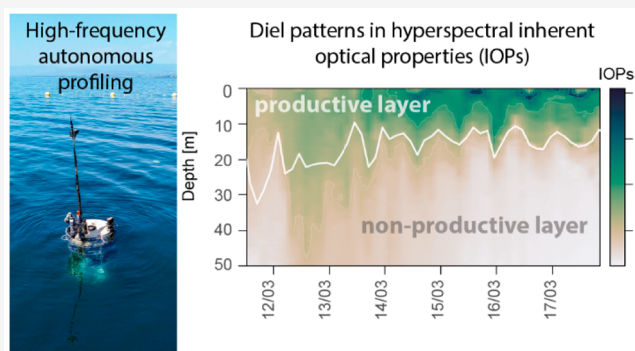
1. INTRODUCTION

Lakes are highly dynamic, heterogeneous systems. Physical and biogeochemical processes that determine surface water quality exhibit spatiotemporal variations over several orders of magnitude.[1] Numerous anthropogenic perturbations generate a range of highly variable aquatic ecosystems responses.[2] This variability can surpass current capabilities for monitoring and interpreting the dynamics of freshwater ecosystems. Small-scale and/or short-term events that govern the long-term trajectory of lake ecosystems especially confound our understanding. Many studies or monitoring programs now use spatially resolved in situ observations such as high-frequency temperature measurements over the entire water column.[3] Fluorescence and dissolved oxygen sensors are also increasingly used in characterizing physical and biogeochemical processes associated with the metabolic dynamics of lake ecosystems.[4,5] Capturing diel-scale temporal variation in dissolved oxygen,[6] the growth and cell division of phytoplankton biomass[7,8] and vertical migration of zooplankton[9,10] has strongly influenced the paradigms that address carbon and nutrient cycling at larger temporal scales. Simultaneous high-frequency measurements of different variables have also contributed to improve our understanding of aquatic ecosystems. For example,

continuous CO_2 and O_2 data have provided key insights into lake metabolism,[11,12] and more generally linked biogeochemical processes (organic matter respiration, photosynthesis, carbonate precipitation, and dissolution) with hydrodynamics and air—water gas exchange.

With the exception of the use of in situ fluorescence sensors to investigate temporal dynamics in phytoplankton,[13−15] high-frequency bio-optical measurements have not been extensively used to study lakes. In contrast, inherent optical property (IOP) measurements, including absorption, attenuation, and scattering have been collected during numerous oceanographic campaigns and by an impressive number of Argo floats or BOUSSOLE buoys equipped with single channel or multi-spectral backscatter-meters or optical transmissometers. These measurements helped establish a better understanding of biogeochemical cycles of the world's oceans,[4,16] and specifically
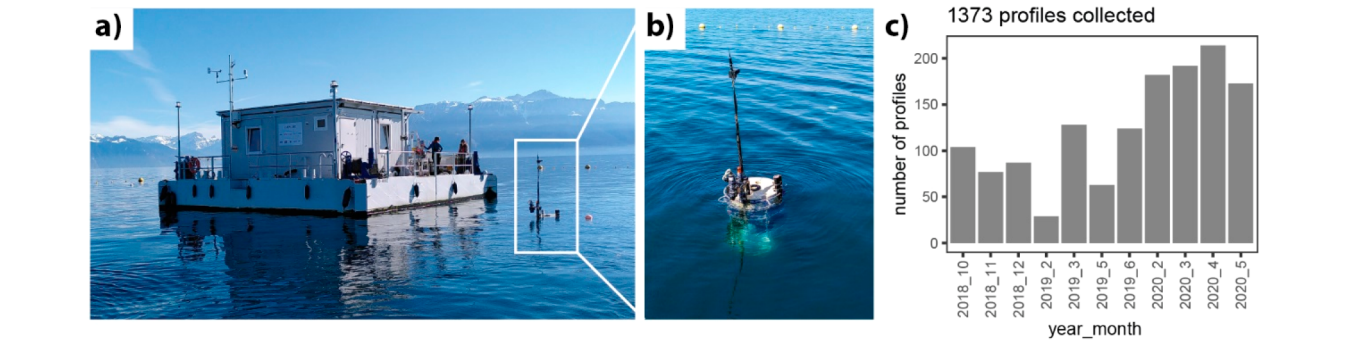
Figure 1. (a) Research platform LéXPLORE with the surfaced Thetis profiler on the right. (b) Close-up of Thetis profiler. (c) Monthly distribution of 1373 Thetis profiles collected from October 2018 to May 2020.

Table 1. List of Thetis Observables and Derived Metrics Reported in This Study (See SI for the Complete Description of Thetis Observations)

	definition	units	derived properties	vertical resolution (cm)
Observables				
Tw	water temperature	°C	density stratification	0.55
PAR	photosynthetically active radiation	μmol m^{-2} s^{-1}	depth of the photic layer	9.8
O_2	dissolved oxygen concentration	mg O_2 L^{-1}	ecosystem production, respiration, mixing and air—water gas exchange	10.6
CHL	chlorophyll-a concentration	μg L^{-1}	phytoplankton biomass	10.0
b700$_{117°}$	scattering at 700 nm observed at 117°	m^{-1}sr^{-1}	suspended particles concentration	10.0
a, c	hyperspectral absorption and attenuation (81 channels from 400 to 730 nm)	m^{-1}		2.2
Derived Metrics				
Z_{ML}	mixed layer depth	m		
Z_{phot}	euphotic depth	m	depth receiving 1% of surface downwelling irradiance	
O_{2sat}	O_2 as percentage of oxygen at saturation	%	ecosystem production, respiration, mixing and air—water gas exchange	10.6
aLH676	absorption line height at 676 nm[30]	m^{-1}	phytoplankton biomass	2.2
c700	attenuation at 700 nm	m^{-1}	particulate organic matter	2.2
Sk	spectral attenuation slope fitted over 300—700 nm spectral range	d.l.	average particle size[7,8]	2.2
bb700	backscattering coefficient at 700 nm	m^{-1}	suspended particles concentration	10.0

elucidated salient temporal and vertical patterns in dissolved and suspended constituents across a broad range of global oceanic conditions.[17−20] In situ hyperspectral IOP measurements not only constrain our understanding of aquatic ecosystems at large, they are also crucial in validating remote sensing optical products.[20] So far, very few studies have used IOP spectrometers to describe physical and biogeochemical processes in lakes.[21,22] The few that exist have detected and described large vertical gradients in lake IOPs. However, the short-term variability of lake water optical properties remains undocumented.

Our objective in this study is to characterize the short-term variability and diel cycles in IOPs and consequently primary production in the surface zones of a large lake, using high-frequency profiler observations. We collected and analyzed 1373 hyperspectral IOP profiles from Lake Geneva (Switzerland−France) between October 2018 and May 2020. This large, high-density data set contains diverse evidence confirming that diel IOPs systematically covary with other quantitative indicators of lake primary production.

2. AUTONOMOUS HIGH-FREQUENCY PROFILING

2.1. Thetis Profiler, Instrumentation, and Deployment. Lake Geneva is a large perialpine lake (maximum depth: 309 m, surface: 580 km^2) located at the border between Switzerland and France. It is oligo-monomictic, and thermal stratification persists from spring to early winter. The deepest seasonal mixing is reached in late winter. Following severe eutrophication in the 1970s primarily due to increasing population on the shorelines with poor wastewater treatment, phosphorus supply to the lake has since been strictly regulated over the past 40 years. Annual mean values of total phosphorus concentration have decreased 4-fold since 1980.[23] Photosynthetic production and phytoplankton biomass, however, did not follow expected trends, which remains a highly debated topic.[6,24,25]

LéXPLORE is a research platform moored in Lake Geneva 570 m offshore and east of the City of Lausanne.[26] It provides a protected open water site for the continuous operation of the Thetis multiparameter autonomous profiler (WetLabs). Thetis was operated on LéXPLORE since October 2018 (Figure 1). The profiler consists of a suite of bio-optical and classical CTD sensors mounted on a positively buoyant frame equipped with an onboard electric winch. The Thetis profiler holds

instruments that measure hyperspectral absorption and attenuation (WetLabs AC-S), scattering at 117° (at 440, 532, 630, 700 nm) and fluorescence by chlorophyll-*a* (EX/EM: 470/695 nm), colored dissolved organic matter (CDOM; EX/EM: 370/460 nm) with WetLabs ECO Triplets BBFL2W and BB3W, hyperspectral downwelling irradiance and upwelling radiance (Satlantic HOCRs), PAR radiation (WetLabs ECO PARS), conductivity, temperature, pressure (Sea-Bird CTD SBE49) and dissolved oxygen (Sea-Bird SBE63). The Supporting Information (SI) contains a complete description of the Thetis payload. When idle, the profiler resides at a fixed parking depth of ∼55 m beneath the photic zone to minimize biofouling. The system profiles every ∼3 h with an ∼8 cm s^{-1} ascending rate. This setting and the battery configuration allow for ∼3 weeks of continuous measurements. Thetis is then recovered, serviced, repowered and redeployed whenever weather conditions permit. All instruments are cleaned before and after each deployment to avoid potential biases due to biofouling. The profiler transmits a subsample of measurements and receives operating commands each time it breaches the lake surface. These communications by telemetry allow near real-time monitoring of the water column. All transmitted data are automatically processed, calibrated, quality controlled, and made accessible online (www.datalakes-eawag.ch). The complete data sets are offloaded manually when the profiler is retrieved for maintenance. Data collected in the first 5 m above the fixed parking depth are discarded to ensure that sensors are flushed and not influenced by the previous profile or by possible deposition of particles during standby.

2.2. Acquired Profiles of Biophysical Variables. This study focused on profile measurements of temperature (Tw, °C), photosynthetically active radiation (PAR, μmol photons m^{-2} s^{-1}), dissolved oxygen (O$_2$, mg L^{-1}), chlorophyll-a (CHL, μg L^{-1}), scattering at 700 nm measured at 117° (b700$_{117°}$, m^{-1} sr^{-1}), and hyperspectral absorption and attenuation (a and c, m^{-1}) (Table 1). We ensured data quality of all Thetis measurements. Observations outside the range of physically possible values for each variable and unrealistic abrupt vertical changes were flagged. Thetis data was regularly compared to multiple overlapping measurements of Tw and O$_2$ collected either manually or with automated sensors and profilers deployed from LéXPLORE. These comparison analyses remained excellent ($R^2 > 0.9$) and stable throughout the period of measurement. Hyperspectral a and c were corrected for temperature, salinity, and backscattering,[27] and quality checked as detailed in the SI.

Several metrics were derived from Tw, PAR, and O$_2$ measurements including mixed layer depth (Z$_{ML}$, m), euphotic depth (Z$_{phot}$, m), oxygen saturation (O$_{2sat}$,%), and Schmidt stability (J m^{-2}). Z$_{ML}$ and Z$_{phot}$ parameters are crucial factors impacting lake biogeochemical cycles. A minimum water column illumination, combined with stratification, causes primary production to become significant near the surface.[28] These factors are expected to impact bio-optical variables. Z$_{ML}$ was taken as the depth where the difference to the uppermost temperature measurement exceeded 0.2 °C. Z$_{phot}$ was calculated as the depth receiving 1% of the average surface irradiance at midday. At the subdaily scale, to account for vertical oscillations caused by internal waves, Z$_{phot}$ was assumed to follow the isotherm corresponding to the euphotic depth at midday. We considered the depth of the productive layer as the largest depth between Z$_{ML}$ and Z$_{phot}$. Oxygen saturation was calculated using the *LakeMetabolizer* R

package[29] as a function of temperature and altitude (here 372 m) and expressed as the percentage of saturation concentration in atmospheric equilibrium to identify periods of photosynthetic production and oxygen accumulation in the water column. Schmidt stability was derived from temperature-based density profiles and lake hypsometry using the *LakeAnalyzer* R package.[29]

The IOP measurements provided estimates of four key metrics (Table 1) including absorption line height at 676 nm (aLH676, m^{-1}), attenuation at 700 nm (c700, m^{-1}), spectral attenuation slope (Sk, dimensionless), and backscattering coefficient at 700 nm (bb700, m^{-1}). Metric aLH676 is a robust indicator for phytoplankton biomass[30,31] computed from bulk spectral absorption[32] after removal of the pure water signal and masking of obvious spectral outliers within the vertical profiles (see SI). Metric c700 is classically used as a proxy for particulate organic matter.[33,34] The spectral attenuation slope, Sk, was extracted by curve-fitting of the attenuation spectra such that $c = k_0 \left(\frac{\lambda}{532}\right)^{-Sk}$, where k_0 (m^{-1}) and λ (nm) are the fitted coefficient and the wavelength, respectively. As documented by several studies, Sk shows a strong negative correlation with the average size of suspended particles.[7,8] Backscattering coefficient bb700 was calculated from b700$_{117°}$ as explained in the SI,[35,36] and closely relates to standard nephelometric turbidity measured at 90° and 780–900 nm.[37]

Additionally, wind speed (U$_5$) and solar radiation were measured 5 m above the lake surface with a Campbell Scientific Automatic Weather Station installed on the LéXPLORE platform and recorded as 10 min averages. These observations were used to investigate the link between in-water variations of physical and bio-optical properties and meteorological events.

We acquired 1373 Thetis profiles over 177 days between 18th October 2018 and 31st May 2020 (Figure 1c). This data set represents an unprecedented density of IOP measurements for a lake, covering all seasons except for late summer (July–September 2019; due to a malfunction in the telemetry system). Both routine and incidental maintenance of the profiler and its sensors resulted in short data gaps (<4 days). The longest contiguous data series with a maximum gap of 2 days was acquired between 11th March and 2nd May 2020 and included 406 profiles.

2.3. Identification of Diel Patterns. When physical and biogeochemical conditions are met, contrasting daytime photosynthesis and ecosystem respiration, as well as losses due to sedimentation and grazing, result in pronounced diel variations in O$_2$ concentrations within the productive zone.[11] Because IOPs are closely linked to the nature of water constituents, in particular to phytoplankton, this study specifically sought to detect high-frequency IOP measurements exhibiting diel variations similar to those observed in O$_2$. To characterize diel signals in the data set, we first extracted average values observed in the productive and nonproductive layers across all profiles and for T_w, O$_2$, aLH676, c700, Sk, and bb700. We then detrended all timeseries by subtraction of a trend component obtained from Empirical Mode Decomposition (R package EMD). We considered the trend as the signal obtained from all variations at frequencies lower than 1/30 h^{-1}. We applied a sinusoidal curve fitting to detrended timeseries $\overline{y}(t)$ for each day comprising more than 5 profiles.
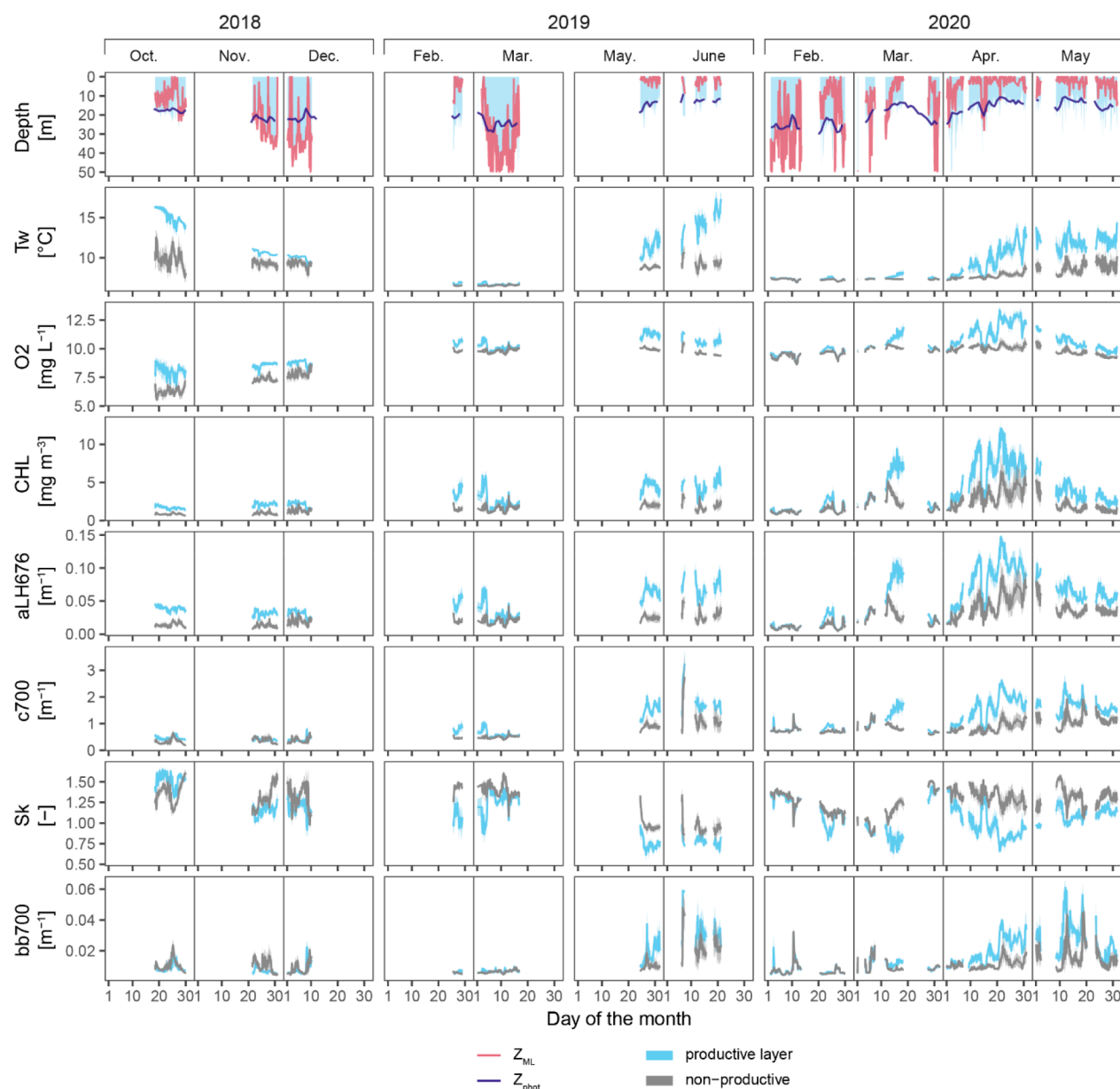
Figure 2. Temporal variations over all 1373 profiles for Z_{ML}, Z_{phot} (upper panel) and for T_w, O_2, CHL, aLH676, c700, Sk, and bb700 in both the productive (blue) and nonproductive (gray) layers.

The expression $\bar{y}(t) = \omega \cdot \cos\left(2\pi \frac{t - \varphi}{t_f}\right)$ is a function of time t (in hours) that can be fitted over all observations available between 6 h before and 6 h after the day considered for the local curve fitting. Coefficients ω, φ, and t_f are model parameters representing the amplitude, phase, and period of the sinusoidal cycle, respectively. The parameter t_f was constrained between 20 and 28 h to account for changes in duration of the photoperiod. Fluorometric CHL was not included in this analysis due to its problematic sensitivity to nonphotochemical quenching (see Section 3.1 and SI Figure S3). Goodness of fit, assessing how well the variables for a given day followed a diel cycle, was based on correlation coefficient (R) between detrended observed and fitted timeseries, and standard deviation of model residuals (σ) normalized by daily median values. We arbitrarily discarded all model fits with $|R| < 0.6$ and $\sigma > 10\%$ of the daily median. All remaining fitted diel cycles were considered suitable for

extracting ω and φ for further analysis. We investigated temporal variations in these two parameters as well as potential links with other variables.

3. SPATIOTEMPORAL PATTERNS IN LAKE OPTICAL PROPERTIES

3.1. Seasonal Patterns. Measurements covered a wide range of lake conditions (Figure 2) from locally fully mixed in winter, to weakly stratified in spring and prominent stratification in summer and fall. Mixed layer depth Z_{ML} appeared in the upper 10 m in spring and deepened as summer stratification developed. Fall cooling pushed Z_{ML} below 30 m depth. Euphotic depth Z_{phot} varied seasonally between ~12 m depth in summer and ~25 m depth in winter. This resulted often in $Z_{phot} > Z_{ML}$ in spring and summer.

The direct comparison of fluorometric CHL with spectrometric aLH676 clearly featured the effect of nonphotochemical
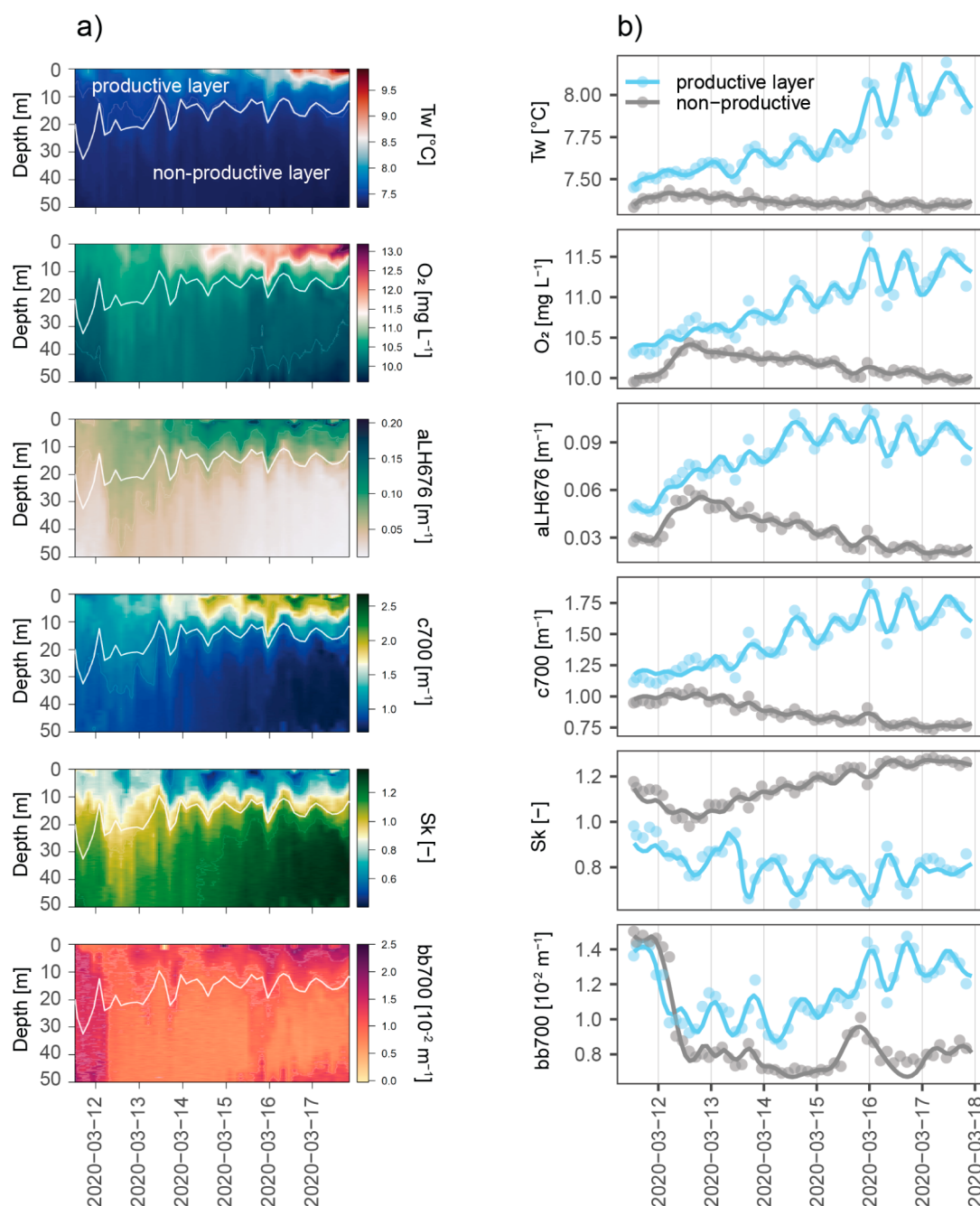
Figure 3. (a) Examples of diel patterns observed in the water column over the period 11th to 17th March 2020 for T_w, O_2, aLH676, c700, Sk, and bb700. White lines separate the productive layer from the nonproductive layer, as explained in Section 2.2. (b) Corresponding average (dots) and model fits (lines) in the productive and nonproductive layers.

quenching (NPQ). Nighttime fluorometric CHL (when PAR irradiance <10 μmol m^{-2} s^{-1}) strongly correlated with aLH676 (R^2 = 0.92, SI Figure S3). The ratio of fluorometric CHL to aLH676 fell during daytime by up to 40%, a direct effect of NPQ near the lake surface.[38] At seasonal time scales, CHL and IOPs covaried closely with thermal and chemical parameters. Spring and summer data showed higher CHL, aLH676, and bb700. Observations in the productive zone generally showed pronounced seasonal variations. The highest CHL value of 14 μg L^{-1} appeared in June 2019 at 10 m depth, in the middle of the productive layer at that time. Attenuation c700 was highly positively correlated to aLH676, and Sk correlated negatively with CHL and aLH676. Metric Sk fell to its seasonal minimum

during spring and summer for periods of significant phytoplankton concentrations as evidenced by systematically lower values in the productive zone relative to those measured below. Metric bb700 followed the dynamic of CHL and aLH676 on seasonal time scales, but also featured short-lived events of higher turbidity unrelated to phytoplankton, as in June 2019 or May 2020.

3.2. Diel Cycles of Lake Optical Properties. An excess of daytime primary production relative to nighttime respiration should create an apparent accumulation of O_2 over several days assuming limited air−water gas exchange and turbulent vertical diffusion. Such a clear production event occurred at several instances in spring and summer, such as between 11th and
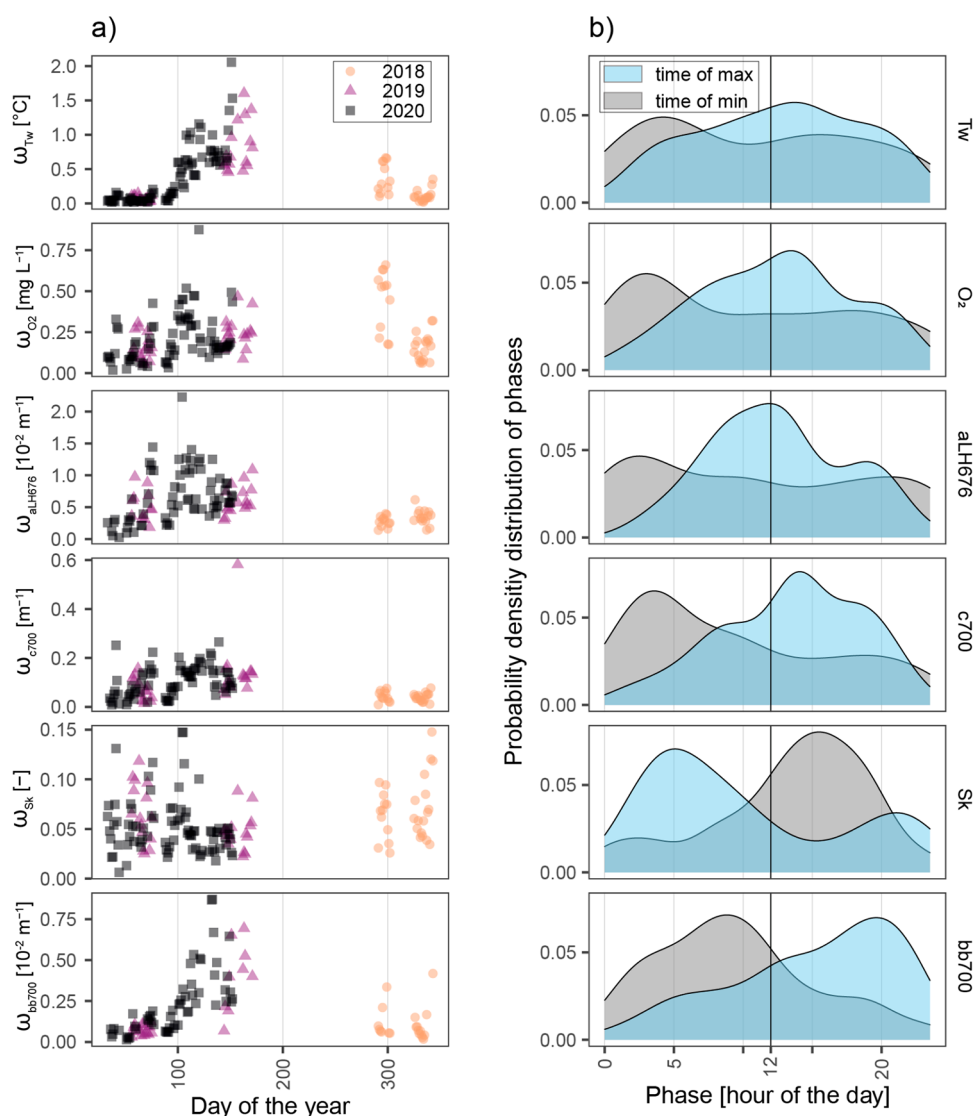
Figure 4. (a) Seasonal variations of the diel amplitudes ω (for Tw, O_2, aLH676, c700, Sk, and bb700) observed in the productive layer. (b) Probability density distributions of the time of daily minima and maxima of all fitted diel cycles observed in the productive layer.

17th March 2020 (Figure 3). During this period, the water column also exhibited near-surface warming from 7.4 to 8.8 °C. Concomitantly, O_2 rose from 10.5 to 12.5 mg O_2 L^{-1}, which corresponded to a change for O_{2sat} from 92 to 113%. The warming alone would cause a slight increase of O_{2sat} by +3.5% which is much smaller than the observed increase of +21%. Concentrations in O_2 also exhibited clear diel patterns with peak-to-peak amplitudes of ~0.4 mg O_2 L^{-1} equivalent to ~3% of the daily median values. These signs of primary production in the productive layer were concomitant with a 200% increase in aLH676, a 130% increase in c700 and a 75% increase in bb700. Meanwhile, Sk decreased by 30%. The IOPs also showed prominent diel patterns. Maxima in T_w and O_2 at the end of the afternoon corresponded to maxima for aLH676, c700, and bb700 and a minimum for Sk. These diel variations represented about 20% of the daily median values for each of the selected IOPs.

Over the entire data set, individual days of measurements conformed well to sinusoidal fitting. Model fits adhered to the acceptance criteria for an average of 93% of cases across all variables within the productive layer. Metric bb700 showed the

lowest degree of fitting with ~73% of the model fits meeting acceptance criteria. Diel amplitudes (ω) varied considerably in time for the different variables (Figure 4a). The largest ω for Tw, O_2, aLH676, c700, and bb700 occurred in spring and summer following expected seasonal patterns in solar irradiance. Metric Sk formed an exception and showed no clear seasonal variation in ω. Phases of these diel cycles were consistent year-round in particular for O_2 and the IOPs (Figure 4b). Water temperature, O_2, aLH676, and c700 tended to be minimal in the morning and peaked in the afternoon. On the contrary, Sk typically was maximal at night between 1 and 5 am, and minimal at the end of daytime. Metric bb700 showed consistent phases, reaching daily minima in the morning and peaking in late afternoon.

Throughout the year, diel amplitudes for the productive zone significantly exceeded those for the nonproductive layer (SI Figure S4). The productive "summer" period exhibited a pronounced vertical gradient in which median ω for the productive zone exceeded that for the nonproductive layer by a factor of 2. Diel amplitudes of IOPs positively correlated to each other and to ω_{O_2} (Figure 5a). For aLH676, c700, bb700,
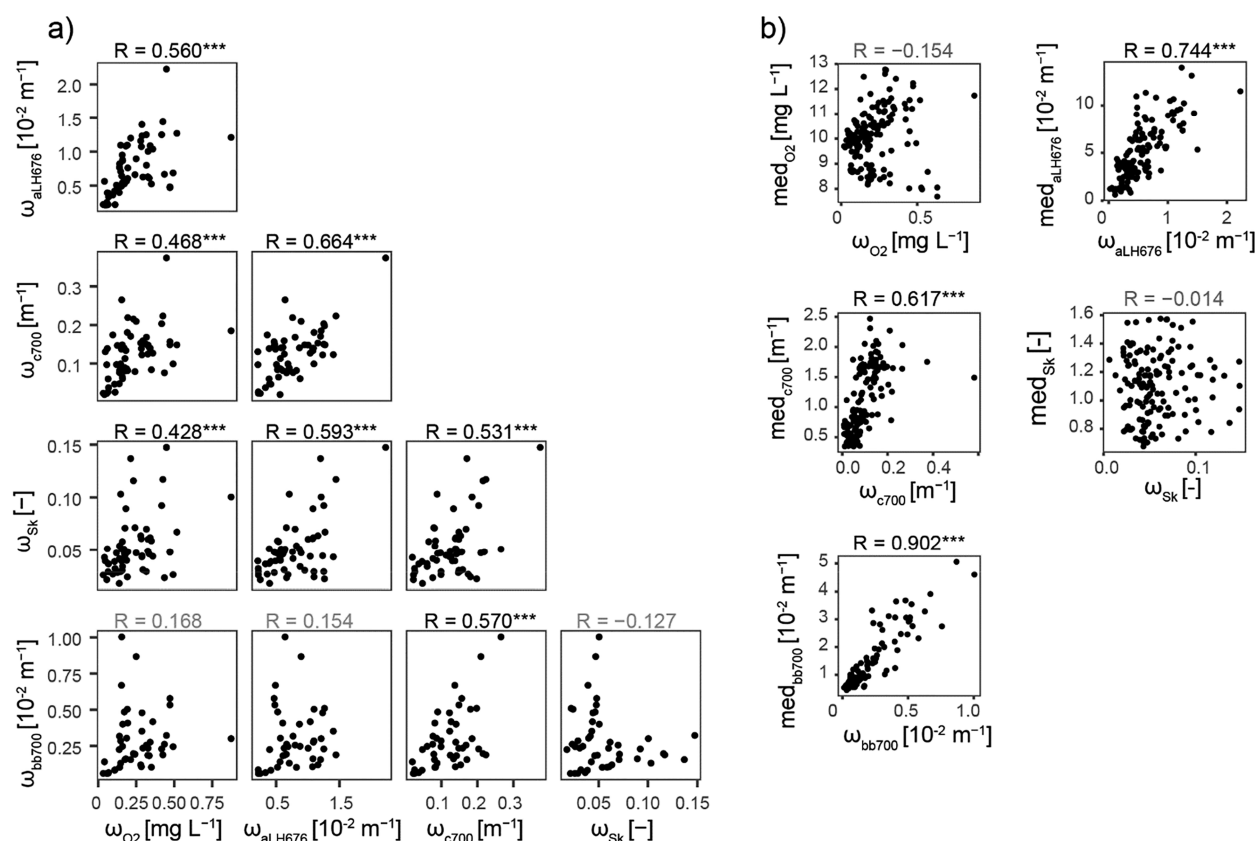
Figure 5. (a) Scatter plot and correlation matrix for diel amplitudes ω of O_2, aLH676, c700, Sk, and bb700 in the productive zone. (b) Relationships between daily median values and diel amplitudes for O2, aLH676, c700, Sk, and bb700 in the productive zone. Correlation coefficients are indicated on top of each scatter plot, and *** highlight statistically significant correlations.

diel amplitudes correlated to the corresponding daily median values, highlighting a direct link between seasonal variations and diel fluctuations. (Figure 5b). For O_2, two opposite patterns emerged in the relationship between daily medians and ω: this correlation was overall linear and positive except for the observations throughout October to December 2018 with an emerging negative correlation. For Sk, there was no sign of correlation between daily median values and diel amplitudes.

Wind intensity appeared as a major driver for diel amplitudes for the IOPs. Throughout April 2020, we acquired Thetis profiles for 26 individual days out of the 30 days. Among them, diel patterns for aLH676 were confirmed for 24 days. This period of intense measurement presented a clear drop in the daily median aLH676 timeseries during short but intense wind events (Figure 6a). Mid-April 2020, three successive wind events occurred in 3 days, largely impacting the water column stability, which dropped by an order of magnitude, and deepened temporarily the extent of the productive zone. This sudden drop in median aLH676 corresponded to particular days when diel patterns were unclear, producing large errors in the sinusoidal fitting at the diel scale, beyond acceptable limits. After this wind event, as soon as stratification was built up again, daily median aLH676 retrieved levels prior to the event. Overall in the entire data set (Figure 6b), the largest ω_{aLH676} were found for daily average U_5 < 3 m s^{-1}, which did not necessarily correspond to the sunniest periods. Similar observations were made for the other IOPs and O_2, with an inverse relationship between diel amplitudes and daily average U_5. The correlation between daily cumulated

solar radiation and diel amplitudes of aLH676 was weak but statistically significant ($R = 0.12$, p-value = 2.8×10^{-5}). Diel amplitudes of aLH676 (and of other IOPs) behaved nonlinearly with the strength of stratification: ω_{aLH676} reached an optimum for Schmidt stability $\sim 2.0 \times 10^3$ J m^{-2}. All in one, these observations indicate the primary role played by wind intensity on the magnitude of the diel patterns for the IOPs at the short-term scale.

4. THE IMPRINT OF PRIMARY PRODUCTION ON LAKE IOPS

High-frequency measurements of lake IOPs showed clear systematic diel fluctuations occurring in the productive zone (Figures 3 and 4). These became especially pronounced during the productive season. Consistent relationships with diurnal O_2 patterns (Figure 5) indicate that IOPs vary systematically with primary production. During the daytime, phytoplankton cells accumulate intracellular carbon by photosynthesis which increases their backscattering cross-section and refractive index.[7,39,40] Respiration and sedimentation rates remain relatively stable throughout day and night,[41,42] but grazing in the surface layers occurs mostly at night due to vertical migration of zooplankton,[10,43] which feed primarily on the largest phytoplankton cells.[44] The combined effects of nighttime respiration, sedimentation, and grazing produce a loss of phytoplankton biomass in the surface layer overnight. This accompanies a gradual shift toward a smaller scattering cross-section until sunrise.[7] Consensus holds that aLH676 and c700 serve as good proxies for chlorophyll-a and particulate organic carbon, respectively. The bb700 metric correlates with
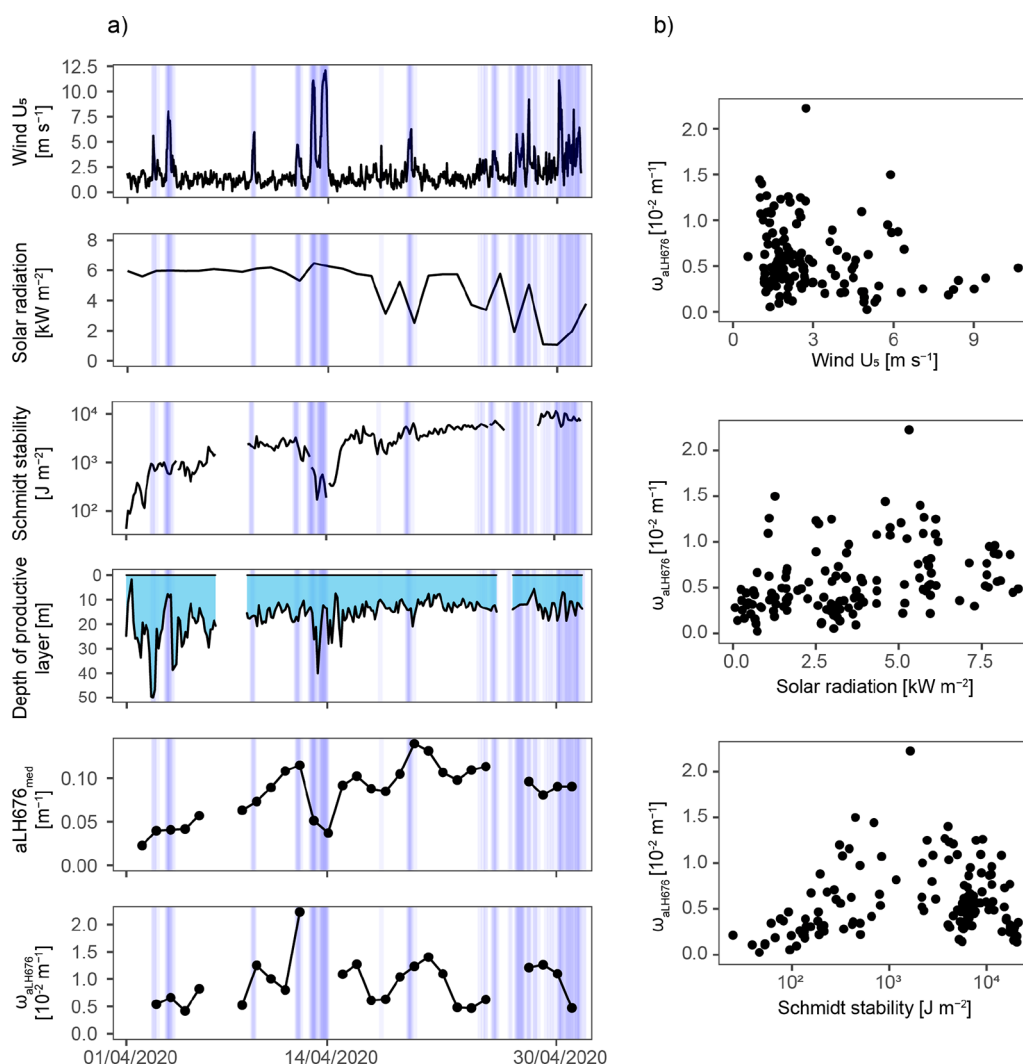
Figure 6. (a) Temporal variations throughout April 2020 of wind speed (hourly U_5), short wave solar radiation (daily cumulated), Schmidt stability, depth of the productive layer, daily median aLH676 in the productive layer, and corresponding diel amplitudes. Blue stripes indicate wind events ($U_5 > 3$ m s^{-1}). (b) Relationships for the entire data set between diel amplitudes of aLH676 in the productive layer and U_5 (top), solar radiation (middle), and Schmidt stability (bottom).

organic suspended matter for instances of high phytoplankton concentrations, and it is likely that diel patterns of bb700 in the photic layer have biological origin. But bb700 is also representative of inorganic and allochthonous particles, possibly interfering with the diel patterns during periods of significant intrusion of turbid riverine inputs,[45] or mobilization of nearshore particulate matter during wind-driven upwelling events.[46] For Sk, the diel patterns we observed correspond to diurnal fluctuations in the average size of phytoplankton cells, with growing sizes over the course of the day (decreasing Sk) and decreasing sizes at night (increasing Sk) due to cells division, loss of the largest cells by sedimentation and grazing.[7] The lack of seasonality in ω_{Sk}, combined with very stable diurnal phases suggests this diurnal change of averge particle size acts independently of the level of phytoplankton biomass. Instead, it is likely reflecting changes in phytoplankton taxonomy that our current database alone cannot explore without regular surveys for species identification and cells size characterization.

The link between diel amplitudes of IOPs and water column stability (Figure 6) highlights the strength of the relationship between lake stratification and primary production. Short-lived

episodic mixing events may either disrupt or enhance production in nutrient-limited systems due to the entrainment of nutrients from deeper layers or nearshore waters.[56,57] The optimum found in the relationship between ω_{aLH676} and Schmidt stability (Figure 6a) likely indicates limiting factors unrelated to stratification, such as nutrients depletion, an increased grazing intensity, or self-shading under the most stable water column condition. Finally, both the median aLH676 and ω_{aLH676} presented occasional decreases that we could not attribute to high winds nor low levels of solar irradiance (e.g., on 22 April 2020, Figure 6). These could also indicate nutrients depletion, grazing, or self-shading, but could as well result from lateral advection of water masses with lower amounts of phytoplankton biomass, which would impact both daily median values and diel fluctuations, as illustrated in Figure 5.

Diel maxima in aLH676 and c700 observed mostly around noon in Lake Geneva did not concur with the phase of the diel cycle exhibited by Sk. The latter consistently reached a minimum around midnight (Figure 4b). An apparent loss of biomass after noon with a gradual increase in particle size after sunset could indicate a decline in the number of the smallest

phytoplankton cells.[52] Possible biological explanations for this could include increasing mortality rates in the afternoon due to photodamage, low nutrient levels hindering phytoplankton cell division once nutrients become depleted,[54,55] and respiration that overcomes production. Overall in the photic zone, a total of 82% of the days that showed an apparent phytoplankton biomass decline in the afternoon also showed a simultaneous decline in O_2 concentration. This likely indicates a shift in net ecosystem production from positive in the morning (production > respiration) to negative in the afternoon (production < respiration). Similar patterns appear in continuous O_2 timeseries at fixed depths but have remained thus far unexplained.[6] Future research should address this question with parallel measurements of O_2, IOPs, particle sizes, carbon, and nutrient concentrations.

Diel changes in IOPs induced by the diurnal behavior of marine phytoplankton have been reported since the late 1980s in oceanographic literature.[47−49] As high-frequency IOP timeseries are becoming more available, researchers have begun interpreting phytoplankton eco-physiological rates directly from IOP measurements.[34,50,51] Relative diel amplitudes of IOPs shown in our analysis represented about 10−20% of daily averages in the productive layer. This is of comparable magnitude to the diel amplitudes shown for backscatter and particulate beam attenuation in previous studies in oceanography.[7,52] Unlike previously reported in the Mediterranean sea,[52] diel patterns for backscatter appeared clearly in Lake Geneva, and presented a strong seasonality. Our work demonstrates the potential use of high-frequency measurements of IOPs for inferring phytoplankton metabolic rates in lakes, as previously shown in oceans. Optically derived metabolic estimates may represent a more robust approach than those which use continuous O_2 measurements. On one hand, a comparative advantage for the former approach may arise due to the dependence of O_2 variations on physical processes such as air−water gas exchange and vertical diffusion, which can be difficult to monitor and constrain.[6,53] On the other hand, changing CHL:C can be difficult to track with IOP measurements alone, and become a significant source of uncertainty for primary production estimates. Yet, because IOP-based primary production estimates apply specifically to phytoplankton rather than overall community rates, parallel measurements of both IOPs and O_2 could offer the possibility of distinguishing contributions from autotrophs and heterotrophs, although in that case, air−water gas exchange must be correctly represented. To account for vertical diffusion and internal baroclinic motion, profiling systems are clearly preferred over continuous fixed-depth measurements.

The combination of tools and expertise will likely provide the key to advance understanding of the carbon cycle in aquatic environments at higher resolution. The unprecedented density of IOP profiles for Lake Geneva calls for approaches that combine frequent IOP measurements with numerical models of lake hydrodynamics and remotely sensed water quality products. Such an approach could elucidate at the scale of the entire lake basin how physical and biogeochemical processes drive the short-term variations of primary production.

■ ASSOCIATED CONTENT

Ⓢ Supporting Information

The Supporting Information is available free of charge at https://pubs.acs.org/doi/10.1021/acs.est.1c02585.

Detailed description of the Thetis autonomous profiler; Figure S1: Detailed view of the WetLabs Thetis profiler operated from the LéXPLORE platform; Table S1: Complete list of instruments and variables measured with the Thetis profiler; Backscattering coefficient from single angle scattering at 117°; Processing and quality control of AC-S data; Figure S2: Flowchart of the AC-S Quality Control (QC) procedure; Figure S3: Relationship between fluorescence-based CHL and aLH676; Figure S4: Range of diel amplitudes in Tw, O2, aLH676, c700, Sk, and bb700 observed in the productive and nonproductive layers (PDF)

■ AUTHOR INFORMATION

Corresponding Author

Camille Minaudo — *Physics of Aquatic Systems Laboratory, Margaretha Kamprad Chair, EPFL, Swiss Federal Institute of Technology, CH-1015 Lausanne, Switzerland;* ⓘ orcid.org/0000-0003-0979-9595; Email: camille.minaudo@epfl.ch

Authors

Daniel Odermatt — *Eawag, Swiss Federal Institute of Aquatic Science and Technology, Surface Waters — Research and Management, CH-8600 Dübendorf, Switzerland; University of Zurich, Department of Geography, CH-8057 Zurich, Switzerland;* ⓘ orcid.org/0000-0001-8449-0593

Damien Bouffard — *Eawag, Swiss Federal Institute of Aquatic Science and Technology, Surface Waters — Research and Management, CH-6047 Kastanienbaum, Switzerland*

Abolfazl Irani Rahaghi — *Eawag, Swiss Federal Institute of Aquatic Science and Technology, Surface Waters — Research and Management, CH-8600 Dübendorf, Switzerland;* ⓘ orcid.org/0000-0003-2703-8319

Sébastien Lavanchy — *Physics of Aquatic Systems Laboratory, Margaretha Kamprad Chair, EPFL, Swiss Federal Institute of Technology, CH-1015 Lausanne, Switzerland*

Alfred Wüest — *Physics of Aquatic Systems Laboratory, Margaretha Kamprad Chair, EPFL, Swiss Federal Institute of Technology, CH-1015 Lausanne, Switzerland; Eawag, Swiss Federal Institute of Aquatic Science and Technology, Surface Waters — Research and Management, CH-6047 Kastanienbaum, Switzerland*

Complete contact information is available at:
https://pubs.acs.org/10.1021/acs.est.1c02585

Author Contributions

C.M. conceptualized the study with supervision by D.O., A.W., and D.B. C.M. and S.L. operated the Thetis autonomous profiler. AIR performed data quality assurance for AC-S measurements. C.M. performed the data analysis and visualization. C.M. and D.O. lead the writing of the manuscript with inputs from all authors.

Notes

The authors declare no competing financial interest.

REFERENCES

(1) Dickey, T. D.; Bidigare, R. R. Interdisciplinary Oceanographic Observations: The Wave of the Future. *Sci. Mar.* **2005**, *69* (S1), 23−42.

(2) Abbott, B. W.; Bishop, K.; Zarnetske, J. P.; Minaudo, C.; Chapin, F. S.; Krause, S.; Hannah, D. M.; Conner, L.; Ellison, D.; Godsey, S. E.; Plont, S.; Marçais, J.; Kolbe, T.; Huebner, A.; Frei, R. J.; Hampton, T.; Gu, S.; Buhman, M.; Sara Sayedi, S.; Ursache, O.; Chapin, M.; Henderson, K. D.; Pinay, G. Human Domination of the Global Water Cycle Absent from Depictions and Perceptions. *Nat. Geosci.* **2019**, *12* (7), 533−540.

(3) Wüest, A.; Lorke, A. Small-Scale Hydrodynamics in Lakes. *Annu. Rev. Fluid Mech.* **2003**, *35* (1), 373−412.

(4) Claustre, H.; Johnson, K. S.; Takeshita, Y. Observing the Global Ocean with Biogeochemical-Argo. *Annu. Rev. Mar. Sci.* **2020**, *12*, 23−48.

(5) Meinson, P.; Idrizaj, A.; Nõges, P.; Nõges, T.; Laas, A. Continuous and High-Frequency Measurements in Limnology: History, Applications, and Future Challenges. *Environ. Rev.* **2016**, *24* (1), 52−62.

(6) Fernández Castro, B.; Chmiel, H. E.; Minaudo, C.; Krishna, S.; Perolo, P.; Rasconi, S.; Wüest, A. Primary and Net Ecosystem Production in a Large Lake Diagnosed From High-Resolution Oxygen Measurements. *Water Resour. Res.* **2021**, *57* (5), No. e2020WR029283.

(7) Dall'Olmo, G.; Boss, E.; Behrenfeld, M. J.; Westberry, T. K.; Courties, C.; Prieur, L.; Pujo-Pay, M.; Hardman-Mountford, N.; Moutin, T. Inferring Phytoplankton Carbon and Eco-Physiological Rates from Diel Cycles of Spectral Particulate Beam-Attenuation Coefficient. *Biogeosciences* **2011**, *8* (11), 3423−3440.

(8) Slade, W. H.; Boss, E. Spectral Attenuation and Backscattering as Indicators of Average Particle Size. *Appl. Opt.* **2015**, *54* (24), 7264−7277.

(9) Burt, W. J.; Tortell, P. D. Observations of Zooplankton Diel Vertical Migration From High-Resolution Surface Ocean Optical Measurements. *Geophys. Res. Lett.* **2018**, *45* (24), 13,396−13,404.

(10) Huber, A. M. R.; Peeters, F.; Lorke, A. Active and Passive Vertical Motion of Zooplankton in a Lake. *Limnol. Oceanogr.* **2011**, *56* (2), 695−706.

(11) Peeters, F.; Hofmann, H.; Fernández, J. E. On the Calculation of Lake Metabolic Rates: Diel O2 and 18/16O Technique. *Water Res.* **2019**, *165*, 114990.

(12) Vachon, D.; Sadro, S.; Bogard, M. J.; Lapierre, J.; Baulch, H. M.; Rusak, J. A.; Denfeld, B. A.; Laas, A.; Klaus, M.; Karlsson, J.; Weyhenmeyer, G. A.; Giorgio, P. A. Paired O2-CO2Measurements

Provide Emergent Insights into Aquatic Ecosystem Function. *Limnol. Oceanogr. Lett.* **2020**, *5* (4), 287−294.

(13) Marcé, R.; George, G.; Buscarinu, P.; Deidda, M.; Dunalska, J.; De Eyto, E.; Flaim, G.; Grossart, H. P.; Istvanovics, V.; Lenhardt, M.; Moreno-Ostos, E.; Obrador, B.; Ostrovsky, I.; Pierson, D. C.; Potužák, J.; Poikane, S.; Rinke, K.; Rodríguez-Mozaz, S.; Staehr, P. A.; Šumberová, K.; Waajen, G.; Weyhenmeyer, G. A.; Weathers, K. C.; Zion, M.; Ibelings, B. W.; Jennings, E. Automatic High Frequency Monitoring for Improved Lake and Reservoir Management. *Environ. Sci. Technol.* **2016**, *50* (20), 10780−10794.

(14) Brentrup, J. A.; Williamson, C. E.; Colom-Montero, W.; Eckert, W.; de Eyto, E.; Grossart, H. P.; Huot, Y.; Isles, P. D. F.; Knoll, L. B.; Leach, T. H.; McBride, C. G.; Pierson, D.; Pomati, F.; Read, J. S.; Rose, K. C.; Samal, N. R.; Staehr, P. A.; Winslow, L. A. The Potential of High-Frequency Profiling to Assess Vertical and Seasonal Patterns of Phytoplankton Dynamics in Lakes: An Extension of the Plankton Ecology Group (PEG) Model. *Inland Waters* **2016**, *6* (4), 565−580.

(15) Pomati, F.; Jokela, J.; Simona, M.; Veronesi, M.; Ibelings, B. W. An Automated Platform for Phytoplankton Ecology and Aquatic Ecosystem Monitoring. *Environ. Sci. Technol.* **2011**, *45* (22), 9658−9665.

(16) Mignot, A.; Ferrari, R.; Claustre, H. Floats with Bio-Optical Sensors Reveal What Processes Trigger the North Atlantic Bloom. *Nat. Commun.* **2018**, *9* (1), 190.

(17) Proctor, C. W.; Roesler, C. S. New Insights on Obtaining Phytoplankton Concentration and Composition from in Situ Multispectral Chlorophyll Fluorescence. *Limnol. Oceanogr.: Methods* **2010**, *8* (12), 695−708.

(18) Boss, E.; Sherwood, C.; Hill, P.; Milligan, T. Advantages and Limitations to the Use of Optical Measurements to Study Sediment Properties. *Appl. Sci.* **2018**, *8* (12), 2692.

(19) Cael, B. B.; Chase, A.; Boss, E. Information Content of Absorption Spectra and Implications for Ocean Color Inversion. *Appl. Opt.* **2020**, *59* (13), 3971.

(20) Brando, V. E.; Dekker, A. G.; Park, Y. J.; Schroeder, T. Adaptive Semianalytical Inversion of Ocean Color Radiometry in Optically Complex Waters. *Appl. Opt.* **2012**, *51* (15), 2808.

(21) Boss, E. S.; Collier, R.; Larson, G.; Fennel, K.; Pegau, W. S. Measurements of Spectral Optical Properties and Their Relation to Biogeochemical Variables and Processes in Crater Lake, Crater Lake National Park, OR. *Hydrobiologia* **2007**, *574* (1), 149−159.

(22) Kalenak, D.; Boss, E.; Effler, S. W. Inherent Optical Properties of Suspended Particulates in Four Temperate Lakes: Application of in Situ Spectroscopy. *Hydrobiologia* **2013**, *713* (1), 127−148.

(23) Tadonleke, R. D.; Lazzarotto, J.; Anneville, O.; Druart, J.-C. Phytoplankton Productivity Increased in Lake Geneva despite Phosphorus Loading Reduction. *J. Plankton Res.* **2009**, *31* (10), 1179−1194.

(24) Krishna, S.; Ulloa, H. N.; Kerimoglu, O.; Minaudo, C.; Anneville, O.; Wüest, A. Model-Based Data Analysis of the Effect of Winter Mixing on Primary Production in a Lake under Reoligotrophication. *Ecol. Modell.* **2021**, *440*, 109401.

(25) Anneville, O.; Dur, G.; Rimet, F.; Souissi, S. Plasticity in Phytoplankton Annual Periodicity: An Adaptation to Long-Term Environmental Changes. *Hydrobiologia* **2018**, *824* (1), 121−141.

(26) Wüest, A.; Bouffard, D.; Guillard, J.; Ibelings, B. W.; Lavanchy, S.; Perga, M.; Pasche, N. LéXPLORE: A Floating Laboratory on Lake Geneva Offering Unique Lake Research Opportunities. *Wiley Interdiscip. Rev.: Water* **2021**, *8* (5), No. e15441.

(27) Pitarch, J.; Volpe, G.; Colella, S.; Santoleri, R.; Brando, V. Absorption Correction and Phase Function Shape Effects on the Closure of Apparent Optical Properties. *Appl. Opt.* **2016**, *55* (30), 8618.

(28) Hopkins, J. E.; Palmer, M. R.; Poulton, A. J.; Hickman, A. E.; Sharples, J. Control of a Phytoplankton Bloom by Wind-driven Vertical Mixing and Light Availability. *Limnol. Oceanogr.* **2021**, *66*, 1953 lno.11734.

(29) Winslow, L. A.; Zwart, J. A.; Batt, R. D.; Dugan, H. A.; Iestyn Woolway, R.; Corman, J. R.; Hanson, P. C.; Read, J. S. Lake-

Metabolizer: An R Package for Estimating Lake Metabolism from Free-Water Oxygen Using Diverse Statistical Models. *Inland Waters* **2016**, *6* (4), 622−636.

(30) Roesler, C.; Uitz, J.; Claustre, H.; Boss, E.; Xing, X.; Organelli, E.; Briggs, N.; Bricaud, A.; Schmechtig, C.; Poteau, A.; D'Ortenzio, F.; Ras, J.; Drapeau, S.; Haëntjens, N.; Barbieux, M. Recommendations for Obtaining Unbiased Chlorophyll Estimates from in Situ Chlorophyll Fluorometers: A Global Analysis of WET Labs ECO Sensors. *Limnol. Oceanogr.: Methods* **2017**, *15* (6), 572−585.

(31) Nardelli, S. C.; Twardowski, M. S. Assessing the Link between Chlorophyll Concentration and Absorption Line Height at 676 Nm over a Broad Range of Water Types. *Opt. Express* **2016**, *24* (22), A1374−A1389.

(32) Roesler, C. S.; Barnard, A. H. Optical Proxy for Phytoplankton Biomass in the Absence of Photophysiology: Rethinking the Absorption Line Height. *Methods Oceanogr.* **2013**, *7*, 79−94.

(33) Cetinić, I.; Perry, M. J.; Briggs, N. T.; Kallin, E.; D'Asaro, E. A.; Lee, C. M. Particulate Organic Carbon and Inherent Optical Properties during 2008 North Atlantic Bloom Experiment. *J. Geophys. Res. Ocean.* **2012**, *117* (6). n/a.

(34) Omand, M. M.; Cetinić, I.; Lucas, A. J. Using Bio-Optics to Reveal Phytoplankton Physiology from a Wirewalker Autonomous Platform. *Oceanography* **2017**, *30* (2), 128−131.

(35) Boss, E.; Pegau, W. S. Relationship of Light Scattering at an Angle in the Backward Direction to the Backscattering Coefficient. *Appl. Opt.* **2001**, *40* (30), 5503−5507.

(36) Boss, E.; Pegau, W. S.; Lee, M.; Twardowski, M.; Shybanov, E.; Korotaev, G.; Baratange, F. Particulate Backscattering Ratio at LEO 15 and Its Use to Study Particle Composition and Distribution. *J. Geophys. Res.* **2004**, *109* (C1), C01014.

(37) ISO 7027-1, 2016; https://www.iso.org/standard/62801.html.

(38) Genty, B.; Briantais, J. M.; Baker, N. R. The Relationship between the Quantum Yield of Photosynthetic Electron Transport and Quenching of Chlorophyll Fluorescence. *Biochim. Biophys. Acta, Gen. Subj.* **1989**, *990* (1), 87−92.

(39) Poulin, C.; Zhang, X.; Yang, P.; Huot, Y. Diel Variations of the Attenuation, Backscattering and Absorption Coefficients of Four Phytoplankton Species and Comparison with Spherical, Coated Spherical and Hexahedral Particle Optical Models. *J. Quant. Spectrosc. Radiat. Transfer* **2018**, *217*, 288−304.

(40) Poulin, C.; Antoine, D.; Huot, Y. Diurnal Variations of the Optical Properties of Phytoplankton in a Laboratory Experiment and Their Implication for Using Inherent Optical Properties to Measure Biomass. *Opt. Express* **2018**, *26* (2), 711−729.

(41) Reynolds, C. S. *The Ecology of Phytoplankton*, Cambridge University Press; Usher, M., Saunders, D., Peet, R., Dobson, A., Eds.; Cambridge, 2006.

(42) Granata, T. C. Diel Periodicity in Growth and Sinking Rates of the Centric Diatom Coscinodiscus Concinnus. *Limnol. Oceanogr.* **1991**, *36* (1), 132−139.

(43) Lorke, A.; McGinnis, D. F.; Spaak, P.; Wuest, A. Acoustic Observations of Zooplankton in Lakes Using a Doppler Current Profiler. *Freshwater Biol.* **2004**, *49* (10), 1280−1292.

(44) Kiørboe, T. How Zooplankton Feed: Mechanisms, Traits and Trade-Offs. *Biol. Rev.* **2011**, *86* (2), 311−339.

(45) Soulignac, F.; Lemmin, U.; Ziabari, S. M. H.; Wynn, H. K.; Graf, B.; Barry, D. A. Rapid Changes in River Plume Dynamics Caused by Advected Wind-driven Coastal Upwelling as Observed in Lake Geneva. *Limnol. Oceanogr.* **2021**, *66* (8), 3116−3133.

(46) Reiss, R. S.; Lemmin, U.; Cimatoribus, A. A.; Barry, D. A. Wintertime Coastal Upwelling in Lake Geneva: An Efficient Transport Process for Deepwater Renewal in a Large, Deep Lake. *J. Geophys. Res.: Oceans* **2020**, *125* (8), 1−18.

(47) Siegel, D. A.; Dickey, T. D.; Washburn, L.; Hamilton, M. K.; Mitchell, B. G. Optical Determination of Particulate Abundance and Production Variations in the Oligotrophic Ocean. *Deep-Sea Res., Part A* **1989**, *36* (2), 211−222.

(48) Stramski, D.; Reynolds, R. A. Diel Variations in the Optical Properties of a Marine Diatom. *Limnol. Oceanogr.* **1993**, *38* (7), 1347−1364.

(49) Briggs, N.; Guemundsson, K.; Cetinić, I.; D'Asaro, E.; Rehm, E.; Lee, C.; Perry, M. J. A Multi-Method Autonomous Assessment of Primary Productivity and Export Efficiency in the Springtime North Atlantic. *Biogeosciences* **2018**, *15* (14), 4515−4532.

(50) Loisel, H.; Vantrepotte, V.; Norkvist, K.; Mériaux, X.; Kheireddine, M.; Ras, J.; Pujo-Pay, M.; Combet, Y.; Leblanc, K.; Dall'Olmo, G.; Mauriac, R.; Dessailly, D.; Moutin, T. Characterization of the Bio-Optical Anomaly and Diurnal Variability of Particulate Matter, as Seen from Scattering and Backscattering Coefficients, in Ultra-Oligotrophic Eddies of the Mediterranean Sea. *Biogeosciences* **2011**, *8* (11), 3295−3317.

(51) White, A. E.; Barone, B.; Letelier, R. M.; Karl, D. M. Productivity Diagnosed from the Diel Cycle of Particulate Carbon in the North Pacific Subtropical Gyre. *Geophys. Res. Lett.* **2017**, *44* (8), 3752−3760.

(52) Kheireddine, M.; Antoine, D. Diel Variability of the Beam Attenuation and Backscattering Coefficients in the Northwestern Mediterranean Sea (BOUSSOLE Site). *J. Geophys. Res. Ocean.* **2014**, *119* (8), 5465−5482.

(53) Peeters, F.; Atamanchuk, D.; Tengberg, A.; Encinas-Fernández, J.; Hofmann, H. Lake Metabolism: Comparison of Lake Metabolic Rates Estimated from a Diel CO_2- and the Common Diel O_2-Technique. *PLoS One* **2016**, *11* (12), No. e0168393.

(54) Olson, R. J.; Vaulot, D.; Chisholm, S. W. Effects of Environmental Stresses on the Cell Cycle of Two Marine Phytoplankton Species. *Plant Physiol.* **1986**, *80* (4), 918−925.

(55) Vaulot, D.; Olson, R. J.; Merkel, S.; Chisholm, S. W. Cell-Cycle Response to Nutrient Starvation in Two Phytoplankton Species, Thalassiosira Weissflogii and Hymenomonas Carterae. *Mar. Biol.* **1987**, *95* (4), 625−630.

(56) Knapp, D.; Fernández Castro, B.; Marty, D.; Loher, E.; Köster, O.; Wüest, A.; Posch, T. The Red Harmful Plague in Times of Climate Change: Blooms of the Cyanobacterium Planktothrix Rubescens Triggered by Stratification Dynamics and Irradiance. *Front. Microbiol.* **2021**, *12* (August), 1−19.

(57) Giling, D. P.; Nejstgaard, J. C.; Berger, S. A.; Grossart, H. P.; Kirillin, G.; Penske, A.; Lentz, M.; Casper, P.; Sareyka, J.; Gessner, M. O. Thermocline Deepening Boosts Ecosystem Metabolism: Evidence from a Large-Scale Lake Enclosure Experiment Simulating a Summer Storm. *Glob. Chang. Biol.* **2017**, *23* (4), 1448−1462.